Imaging of Subsurface Objects Using Resonant Seismic Emission

Valeri Korneev, Lawrence Berkeley National Laboratory*
Evgeny Landa, OPERA

Summary
Shallow subsurface objects with strong contrasts (such as tunnels, caves, pipes, filled pits etc) are capable of generating strong primary scattered waves, which are customly recognized as a main information carrying signals. However, detection and interpretation of those signals are heavily compromised by strong interfering noise coming from direct waves, groundroll and scattering from other subsurface heterogeneities. If our objects of interest are capable to carry waves with velocities which are slower than in the embedding medium the seismic energy can be trapped in forms of circumferential waves and than can be slowly released long after the initial impact. Release of trapped energy mostly happens as a resonant emission of shear waves and can be detected in forms of sharp resonant peaks at single records. Resonant emissions have characteristic quasi-hyperbolic traveltime patterns on single shot gathers. Inversion of these patterns allows accurate imaging of object locations, while values of resonant frequencies have direct relationship with object sizes. Imaging can be done at single frequency when no accurate information about source initiation time is needed and strong direct and primary scattering waves are simply muted. All the conclusions are supported by the results of modeling and field data.

Introduction
Imaging of shallow subsurface heterogeneities has a variety of important applications. Those applications include detection and location of tunnels of different kind, pipes, buried containers, UXOs, mine shafts etc. Being very contrast scatterers, these objects are capable to generate strong scattered waves where primary PP, PS, SS waves carry away most of the energy which was brought by the incident waves. This conclusion follows from numerical and analytical results obtained from canonical solutions for the sphere and cylinder (e.g. Korneev and Johnson, 1996) and practically all the efforts in determining underground scatterers, rely on utilization of these waves (e.g. Landa and Keydar, 1998). For both high- and low- velocity objects the primary scattered waves have the same order of magnitude. The main difference between these group of objects is in later arrivals which still exist at times when all the primary waves are already passed. While high-velocity objects effectively radiate most of the energy soon after the impact, the low-velocity objects trap some fraction of energy in the form of circumferential waves (Hassan and Nagy, 1997) which propagate rotating along the interface between the object and the embedding medium. Circumferential waves include surface Rayleigh-type waves (propagating mostly in the embedding medium), Stoneley waves (propagating mostly in the fluid, if present), Frantz waves (body waves trapped in the object because of its curvature). Strong impedance contrast ensures small radiation losses for circumferential waves and they slowly decay in amplitude while rotating inside/around the object. Some circumferential waves exist in the high-velocity objects but their amplitudes decay very fast because of strong radiation in outer medium.
Most of the secondary (formed by multiples) scattered energy propagates as shear waves. This follows from canonical solutions and reflects the fact that S- waves are slower than P-waves and that energy conversion is generally larger for slow velocity waves. In practice, the amplitudes ratio for S to P- waves is increased even more because the local amplification factors are inversely proportional to wave velocities. Possibility of neglecting P- waves in late scattering arrivals simplifies imaging as it will be demonstrated for the field and modeled data.
In practice, there are several classes of objects which contain elements with velocities lower than in embedding media.. These are tunnels, pipes and cavities filled with gas (air). Low gas densities in such structures result in long-living circumferential waves (primarily of the Stoneley type). Generally, water and other underground liquids (oil) have comparatively low velocity of about 1500 m/s and being contained in some volume can trap energy. At the same time, in very shallow subsurface the embedding media can have velocities equal to just few hundreds m/s, which is much lower than typical velocities in a liquid, where liquid-containing objects lose their energy trapping capabilities. This, however might not be the case when liquid contains some gas bubbles and such mixture has compressibility of gas and density of liquid. Such parameter combination, leads to very low propagation velocities (Kaelin, 1998) which can be lower than those in embedding shallow subsurfaces. Another class of wave trapping objects are localized low-velocity zones, which can have naturally low velocity (like a part of a coal seam) or which result from some impact such as filled excavation pits where loosened rock/soil have smaller elastic modules compare with embedding medium. In the latest case, an intrinsic attenuation inside of the object contributes to the rate of wave amplitude decrease.

Field data
The filed experiment was conducted in 1999 aimed to generate a test data set for the methods of subsurface object detection and imaging. Soil was a compacted consolidated sand with P- velocity of 500 m/s and S- velocity of 240 m/s. The object was a water-filled barrel having 60 cm in

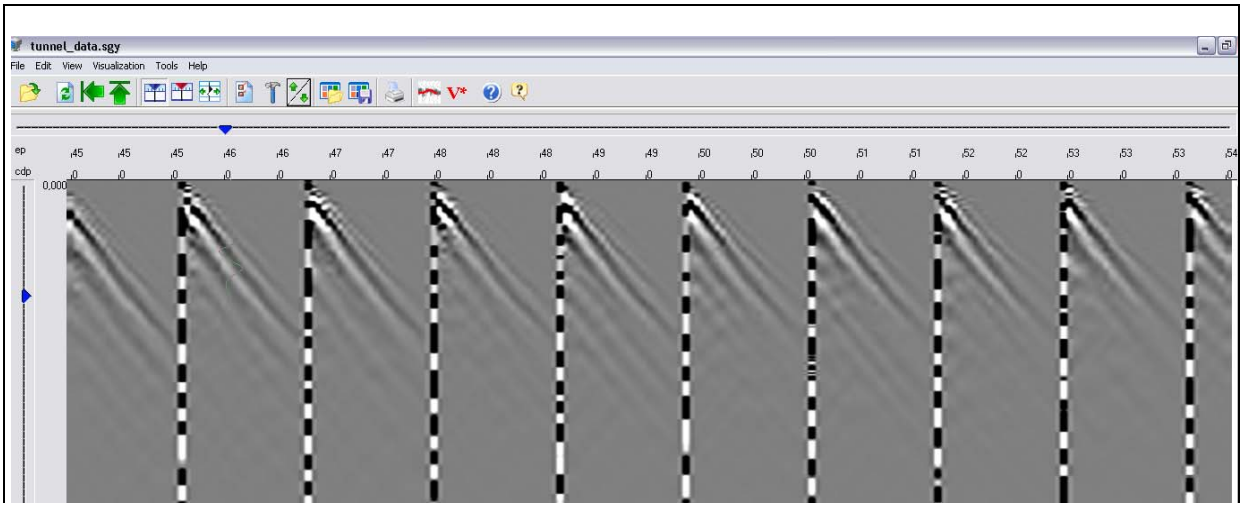

Figure 1. Shot gathers for field data recorded above the buried barrel. Visible is the direct S-wave.

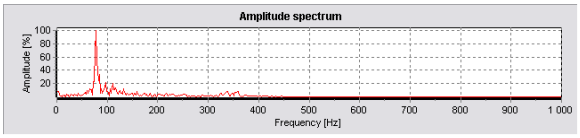

Figure 2. Amplitude spectrum of AGCd late arrivals has sharp peak at 78 Hz.

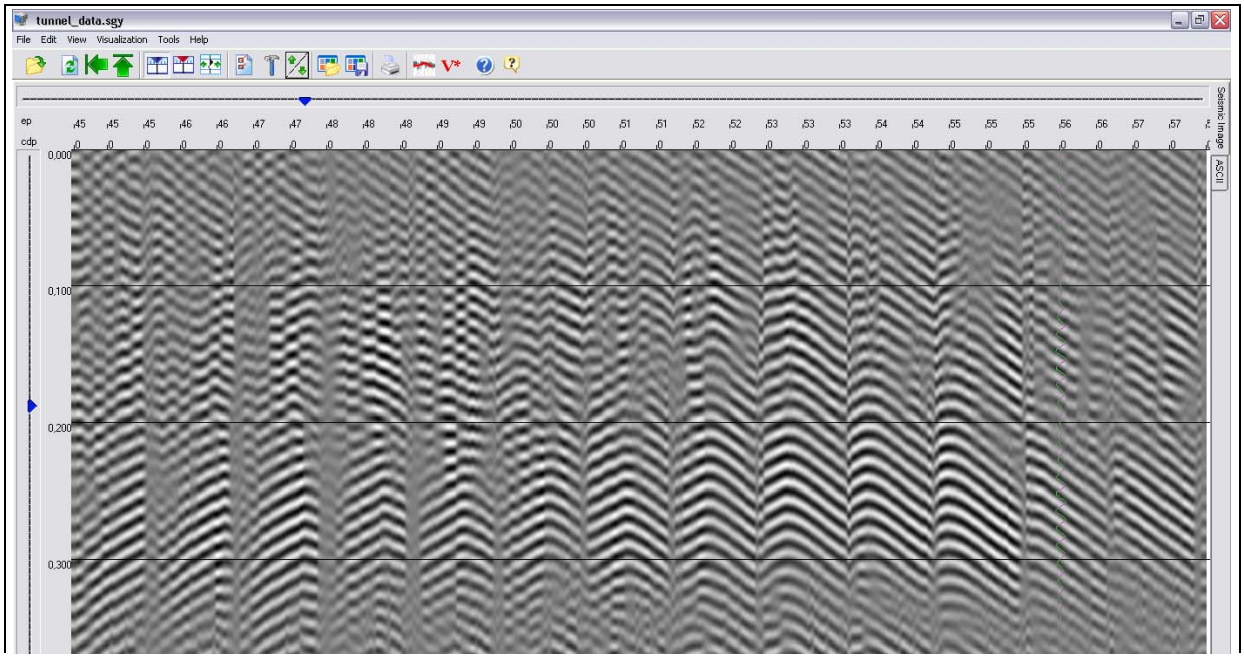

Figure 3. Shot gathers after AGC and band-pass filtering around 78 Hz show hyperbolic signatures of a secondary source.

diameter and 120 cm in height. Some air bubbles were left inside of the barrel before it was sealed. The barrel was placed at 5-6 meter depth in a specially excavated pit which was then filled back with soil. A 24-channel 0.5 m spaced line of vertical geophones was used for every ground shot made by a sledge-hummer. The shot point was positioned at the first receiver of each line. There were 87 shots in total with 1 m spacing interval. The middle receiver of the line #51 was directly above of the barrel. Records were 0.5 s in length with 0.5 ms data sampling rate. Figure 1 shows raw shot gathers #48-53. After applying automatic gain control (AGC) the late (0.25-0.5 ms) interval revealed sharp resonant peaks in amplitude spectra at 78 Hz (Figure 2). Band-pass filtering of traces in the 75-83 interval gave clear signature of a secondary seismic source with apex in the middle of the line 51 (Figure 3). Note that the phase slopes (240 m/s) of the secondary source correspond to velocities V_S of shear waves in embedding medium. Result of migration of data from Figure 3 is shown on Figure 4 giving accurate location for the barrel.

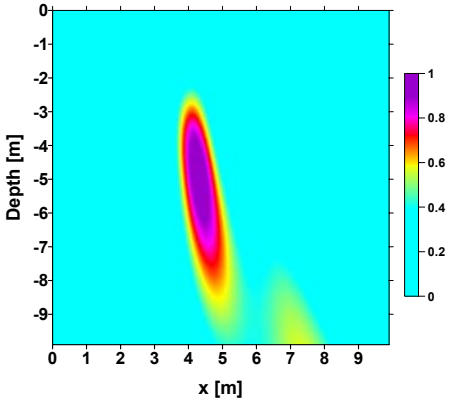

Figure 4. Migrated image of buried barrel.

The imaging was performed after picking the phases by applying a migration-type transformation of the form

$$S(x,z)=\sum_j\left|\sum_k \exp\left(i2\pi f_0\left[r_{jk}(x,z)/v_s-\tau_{jk}\right]\right)\right| \quad (1)$$

where indexes j and k correspond to respectively to sources and receivers, f_0 is the resonant frequency, $r_{jk}(x,z)$ are the distances from receivers to an image point. Wave traveltimes τ_{jk} are picked from the pre-processed data (Figure 3) following the same phase and assigning zero value to a reference trace. Note that the field S is invariant to addition of an arbitrary constant to time picks τ_{jk} for any source index *j*, and, therefore, no information about source triggering and location is needed.

Fitting a first resonant peak for a liquid-filled sphere with radius R=0.3 cm gave fluid velocity 70 m/s which is consistent with Kaelin, (1998) for fluid with air babbles model with 1 g/cm^3 density (Figure 5).

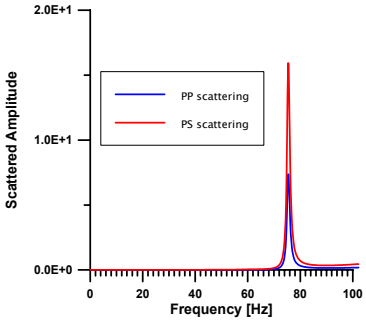

Figure 5. Scattering cross-section for fluid-filled sphere

Modeling

We modeled the field data with 2D finite-difference code using 40x 12.5 m model with 0.05 m grid spacing. Background Vp and Vs velocities had same values as in the field experiment. Local object was modeled as a 1m x 1 m rectangular containing liquid with 70 m/s velocity and 1 g/cm^3 density. Ten shot gathers were computed using 3 m spacing for sources. The surface receiver line was the same for all shots and had 61 sensors separated by 0.5 m. Single shot gather for the shot #3 is shown on Figure 6, where similar to the field case primary scattered waves rapidly decay after 0.2 s. The recording length was 1 s.

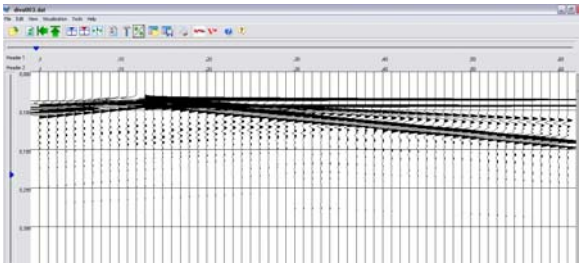

Figure 6. Single shot gather for modeled field

Snapshot image at 0.3 s (Figure 7) shows that at later time the propagating field is predominantly comprised of shear waves caused by circumferential waves in the object.

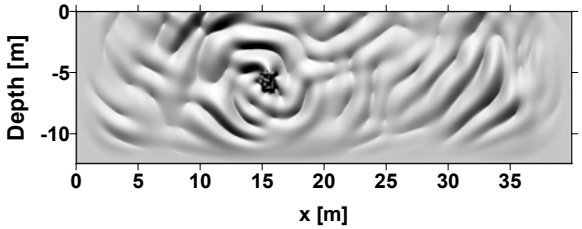

Figure 7. Snap-shot shows propagation of circumferential waves along the object.

Spectral content of the late parts of the records(after 0.5 s) shows the presence of sharp peak at 53 Hz in all traces (Figure 8).

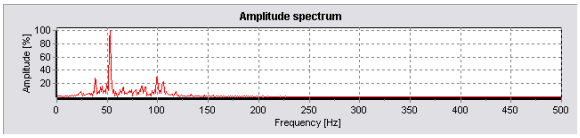

Figure 8. Amplitude spectrum of AGCd late arrivals has sharp peak at 53 Hz.

All the data were AGCd and band-pass filtered around the peak frequency leading to the images like shown on the Figure 9 and revealing the wave structure similar to the one on real data (Figure 3).

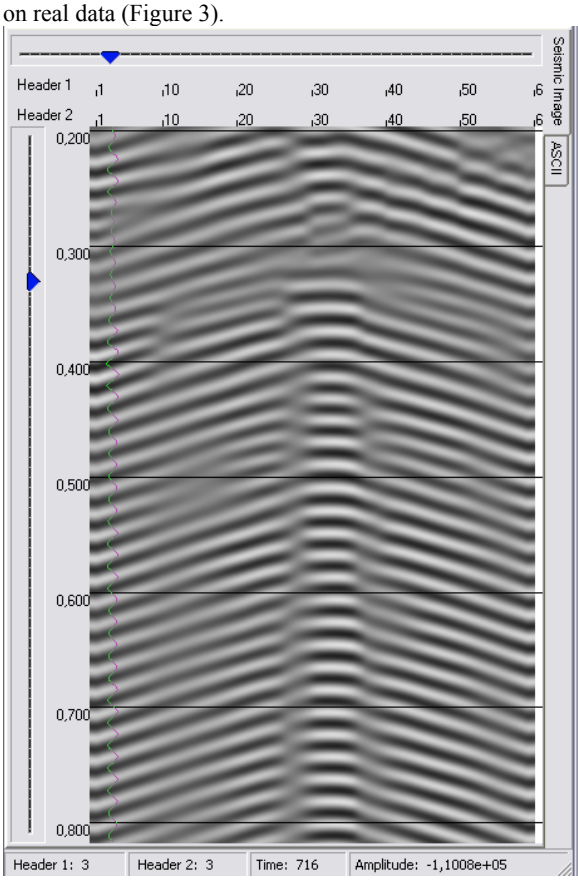

Figure 9. Late arrivals of modeled data after AGC and band pass filtering around the resonance frequency have repeating quasi-hyperbolic pattern similar to one observed for field data (Figure 3).

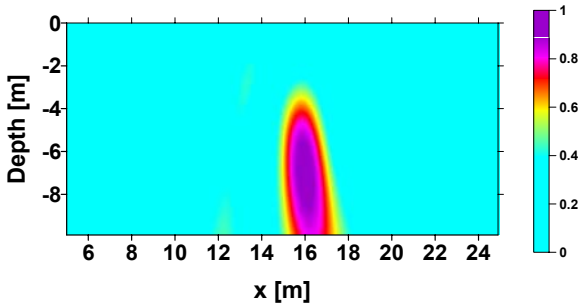

Figure 10. Migrated image of the modeled object is similar to one obtained from field data. (Figure 4).

Conclusions

Low-velocity subsurface heterogeneities trap seismic energy and capable to release it long after the recordings of primary scattered waves. Trapped energy primarily consists of circumferential waves propagating along the perimeter of the object and radiates in the surrounding medium as body waves. Circumferential waves propagate in both directions around the object which potentially can create discontinious traveltime curves. Most of the energy irradiated back to the embedding medium is carried by shear waves. This simple data pattern makes it attractive candidate for inversion techniques based on migration (backpropagation) principles. Contrary to conventional diffraction imaging techniques, the resonant emission imaging can be performed at single frequencies and does not require accurate information about source position. There is also no need in laborious wave-separation pre-processing because all primary waves can be simply muted. It is expected that multiple objects can be detected and imaged using separation in frequency domain. It is clear that exact timing of the source excitation is not important and trapped energy radiation can possibly be observed in the presence of the background noise, leading to cost effective object detection techniques. Requirements to the sensor coverage are yet to be estimated. Overall, the new object detection method is proposed, which shows good correspondence between field and modeled data. In its current formulation the method is ready for extensive testing and tuning.

Acknowledgments

This work was supported by the National Energy Technology Laboratory, Office of Fossil Energy Sciences, of the U.S. Department of Energy under Contract No.DE-AC03-76SF00098. Authors thank GeoKinetiK LLC for providing Seismic Office software. Field data were provided by GII. . The authors would like to thank TOTAL for sponsoring this work. OPERA is a private organization funded by TOTAL and supported by the Pau University.